第 28 卷第 9 期
2012 年 9 月

无 机 化 学 学 报
CHINESE JOURNAL OF INORGANIC CHEMISTRY

Vol.28 No.9
1935-1939

NASICON 结构的锂离子导电微晶玻璃结构与电导率

何 坤* 王衍行 祖成奎 刘永华 马眷荣

(中国建筑材料科学研究总院石英与特种玻璃研究院,北京 100024)

摘要: 通过对 $Li_xAl_{x-1}Ge_{3-x}(PO_4)_3$($x$=1.1~1.9)锂离子导电玻璃的差示量热扫描(DSC)数据,结合 XRD 及其 Rietveld 精修、FESEM 和交流阻抗等测试方法,研究了该系微晶玻璃的物相组成、主晶相晶胞参数变化情况、微观结构形貌、锂离子电导率和电化学窗口等。结果表明:$Li_xAl_{x-1}Ge_{3-x}(PO_4)_3$($x$=1.1~1.9)锂离子导电微晶玻璃析出导电主晶相为 $LiGe_2(PO_4)_3$。当 x=1.5 时,由于导电主晶相 $LiGe_2(PO_4)_3$ 晶粒充分长大、分布均匀,晶界清晰,LAGP 导电微晶玻璃的室温电导率最高(可达 5.3×10^{-4} S·cm^{-1}),电化学窗口为 7.2 V,可以满足全固态锂离子电池对电解质高室温电导率和宽电化学窗口的应用要求。

关键词: 微晶玻璃; 固体电解质; Rietveld 精修; 离子电导率

中图分类号: O753$^+$.1; PM191 **文献标识码**: A **文章编号**: 1001-4861(2012)09-1935-05

Crystal Structure and Ionic Conductivity of the NASICON-Type Lithium Ion Conducting Solid Electrolyte

HE Kun* WANG Yan-Hang ZU Cheng-Kui LIU Yong-Hua MA Juan-Rong

(*Institute of Quartz and Special Glasses, China Building Materials Academy, Beijing* 100024 *China*)

Abstract: The $Li_xAl_{x-1}Ge_{3-x}(PO_4)_3$ (x=1.1~1.9) solid solutions were prepared as glass ceramics pellets. The title compounds crystallize in the NASICON (Na Super Ionic Conductor), R3c type structure, space group, and the crystal structures were characterized by the Rietveld method with laboratory powder diffraction data. The annealed glasses and glass ceramics were also characterized by DSC, FESEM and AC Impedance techniques. The results indicate that the major phase of the glass ceramics is $LiGe_2(PO_4)_3$, with $AlPO_4$ and $Li_4P_2O_7$ as the side-phases for some samples. Additionally, the highest total ionic conductivity (5.3×10^{-4} S·cm^{-1}) at room temperature is obtained when x=1.5 for $Li_xAl_{x-1}Ge_{3-x}(PO_4)_3$ glass ceramics, with homogeneous crystals distribution and wide electrochemical window (7.2 V).

Key words: glass ceramics; solid electrolyte; Rietveld renement; ionic conductivity

0 Introduction

In comparison with the parent glass, glass ceramics demonstrate a denser microstructure, less grain boundary effects and better chemical stability. Moreover, the NASICON (Na Super Ionic Conductor) structures glass ceramics exhibit higher ionic conductivity than the corresponding mother glasses when conductive crystals are precipitated from the glasses. These glass ceramics have been attracted much attention owing to their excellent lithium ionic conductivity and low atomic mass of lithium. Lithium ionic conductors stood a good chance to be used as electrolytes for all solid state lithium ionic batteries[1-3].

收稿日期:2012-02-24。收修改稿日期:2012-04-09。

国家自然科学基金(No.60808024).资助项目。

*通讯联系人。E-mail:cbmahekun@163.com

These lithium ionic conducting glass ceramics are usually obtained by sol-gel process [4-5], the classical powder sintering route [6-7] and glass-ceramic processes [8-10]. Since homogeneous microstructures and high lithium ionic conductivity, the last method is extensively used to fabricate lithium ionic conducting glass ceramics. Based on the high lithium ionic conductivity and excellent stable with lithium metal, lithium aluminum germanium phosphate (LAGP) glass-ceramic is immensely attractive as electrolyte in lithium ionic battery. Consequently, the structural and electrical properties of LAGP glass ceramics are dependent on the content of Li_2O. Therefore, it is essential to study the chemical composition on crystals microstructure and conductivity of LAGP glass ceramics.

The aim of the present work is to investigate the effect of various Li_2O contents on the thermal properties, crystal structural changes, micro structures and conductivity of LAGP glass ceramics.

1 Experimental

A glass batch [$Li_xAl_{x-1}Ge_{3-x}(PO_4)_3$, x=1.1~1.9] comprised of reagent grade chemicals such as Li_2CO_3, Al_2O_3, GeO_2 and $NH_4H_2PO_4$ was prepared. The aforementioned chemicals weighed, mixed, and milled in a high energy milling machine for 60 min to homogenize. Then they were transferred to an electric furnace and heated in an alumina crucible at 973 K for 2 h in order to decompose ammonia, carbon dioxide gases and water vapor out from the starting materials. Then, they were heated to 1723 K and melted at the temperature for 2 h and then poured onto preheated stainless steel plates. The cast glass sheets were annealed at 723 K for 2 h to release the thermal stresses and then allowed to cool to room temperature. The samples were subsequently crystallized at 1 123 K for 8 h.

Thermal stabilities were analyzed by differential scanning calorimetry (DSC, Netzsch STA 449C, Waldkraiburg, Germany) for the fine-powdered glass heated to 1000 K from room temperature at a rate of 10 K·min^{-1}. The X-ray diffraction (XRD) investigations were conducted by a D-max-RB Model diffractometer using Cu $K\alpha$ radiation (λ=0.154 18 nm) at 40 kV and 40 mV settings in the 2θ range from 10° to 80°. The microstructures morphology of the formed crystal was characterized by field emission scanning electron microscopy (FESEM) (model Supra 55VP). The ionic conductivities were determined using impedance spectroscopy (Solartron 2016 impedance analyzer) in the 0.1 ~10^6 Hz frequency range with voltage amplitude of 500 mV.

2 Results and discussion

Fig.1 shows DSC plots of the air-quenched glasses of $Li_xAl_{x-1}Ge_{3-x}(PO_4)_3$ (x=1.1~1.9). The glass transition (T_g) and crystallization (T_c) temperatures of the parent glass were estimated for all samples. The sharp crystallization peaks in Fig.1 indicate a rapid crystallization process for all the samples. It can be seen that T_c increases gradually with the increasing x, suggesting that the crystallization of the glasses is more and more difficult. Table 1 lists the values of T_g, T_c, and ΔT(ΔT=T_c−T_g) of the glass samples. It is clear that increasing the x from 1.1 to 1.9 results in an increase in ΔT, suggesting the enhanced thermal stability of the glass.

To identify the possible phases crystallized during the heat treatments of LAGP glass, XRD patterns were recorded for $Li_xAl_{x-1}Ge_{3-x}(PO_4)_3$ (x=1.1~1.9). The NASICON-type phase of $LiGe_2(PO_4)_3$ is the dominant crystal phase in $Li_xAl_{x-1}Ge_{3-x}(PO_4)_3$ (x=1.1~

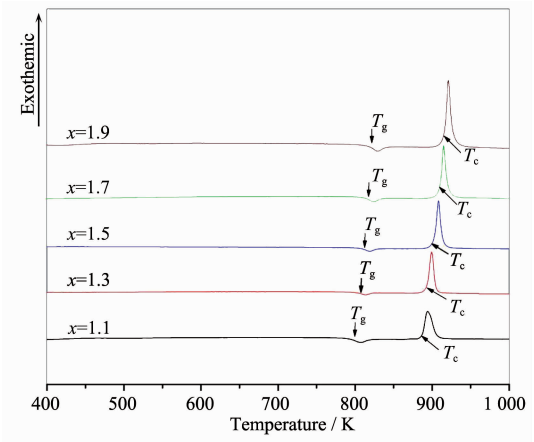

Fig.1 DSC plots of $Li_xAl_{x-1}Ge_{3-x}(PO_4)_3$ (x=1.1~1.9) glass samples

Table 1　Glass transition (T_g) and crystallization (T_c) temperatures for $Li_xAl_{x-1}Ge_{3-x}(PO_4)_3$ (x=1.1~1.9) glasses system

x	T_g / K	T_c / K	ΔT / K
1.1	790.4	876.2	85.8
1.3	796.2	880.3	84.1
1.5	801.5	888.3	86.8
1.7	807.4	896.6	89.2
1.9	809.1	900.4	91.3

1.9) glass ceramics system, with $AlPO_4$ and $Li_4P_2O_7$ as the side-phases for some samples. Based on the parameters of $LiGe_2(PO_4)_3$, $Li_4P_2O_7$ and $AlPO_4$ phases from Inorganic Crystal Structure Database (ICSD), Rietveld rening was made by Material Analysis Using Diffraction (MAUD) software. The unit cell parameters and R-agreement Rietveld factors are given in Table 2 for the full series. The weight fractions each phase are also shown in Table 2.

Table 2　Crystallographic parameters for $Li_xAl_{x-1}Ge_{3-x}(PO_4)_3$ and side-phase content, $AlPO_4$ and $Li_4P_2O_7$ from Rietveld studies

Li content x	Relative weight fraction / wt%			Lattice parameters of $LiGe_2(PO_4)_3$			Refning agreement factor R_w / %
	$LiGe_2(PO_4)_3$ (±0.1%)	$Li_4P_2O_7$ (±0.1%)	$AlPO_4$ (±0.1%)	a (±0.000 2 nm)	c (±0.000 2 nm)	V (±0.000 4 nm^3)	
1.1	98.4	—	1.6	0.825 0	2.067 7	1.200 1	11.32
1.3	96.1	—	3.9	0.825 5	2.052 6	1.203 3	12.21
1.5	96.0	—	4.0	0.827 6	2.039 4	1.209 7	9.83
1.7	95.1	2.3	2.6	0.829 7	2.059 2	1.227 7	10.21
1.9	91.1	6.4	2.5	0.831 5	2.047 9	1.234 9	11.33

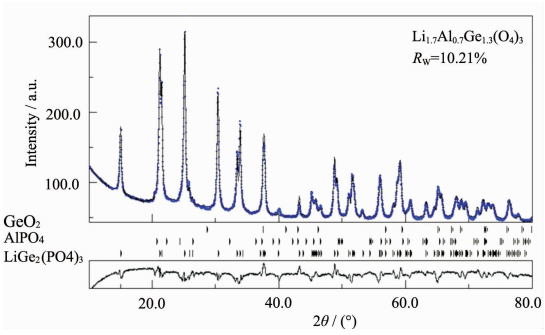

dot line: experimental points; solid line: renement

Fig.2　Rietveld renement of the XRD patterns for $Li_xAl_{x-1}Ge_{3-x}(PO_4)_3$ (x=1.7) glass ceramic crystallized at 1 123 K for 8 h

It can be seen in Table 2 that the a-axis parameters and volume increase steadily along the series, which is probably caused by the incorporation of a part of the excess lithium into the $LiGe_2(PO_4)_3$ structure. As an indication of Rietveld renement quality, the difference plot for the observed and calculated patterns for the sample x=0.7 is shown in Fig.2. The rening agreement factor of R_w is reliable when R_w<15%[11-12].

The typical FESEM images of $Li_xAl_{x-1}Ge_{3-x}(PO_4)_3$ (x=1.1~1.9) glass ceramics are shown in Fig.3 after crystallization at 1123 K for 8 h. As shown in Fig.3 (a), a few grains could be observed in the $Li_{1.3}Al_{0.3}Ge_{1.7}(PO_4)_3$ sample due to low content of Li_2O. Interesting microstructure changes are observed in $Li_{1.5}Al_{0.5}Ge_{1.5}(PO_4)_3$ and $Li_{1.7}Al_{0.7}Ge_{1.3}(PO_4)_3$ glass ceramics, as shown in Fig.3(b) and Fig.3(c). With the average grain size of about 90 nm, the homogeneous microstructures of LAGP glass ceramics indicate that sufficient content of Li_2O promote the growth of crystals during crystallization process. However, lesser crystals can be observed in $Li_{1.9}Al_{0.9}Ge_{1.1}(PO_4)_3$ glass-ceramic (Fig.3(d)). These FESEM observations illustrate that the content of Li_2O should be 1.5 to 1.7 in $Li_xAl_{x-1}Ge_{3-x}(PO_4)_3$ (x=1.1~1.9) glass ceramics in order to achieve homogeneous

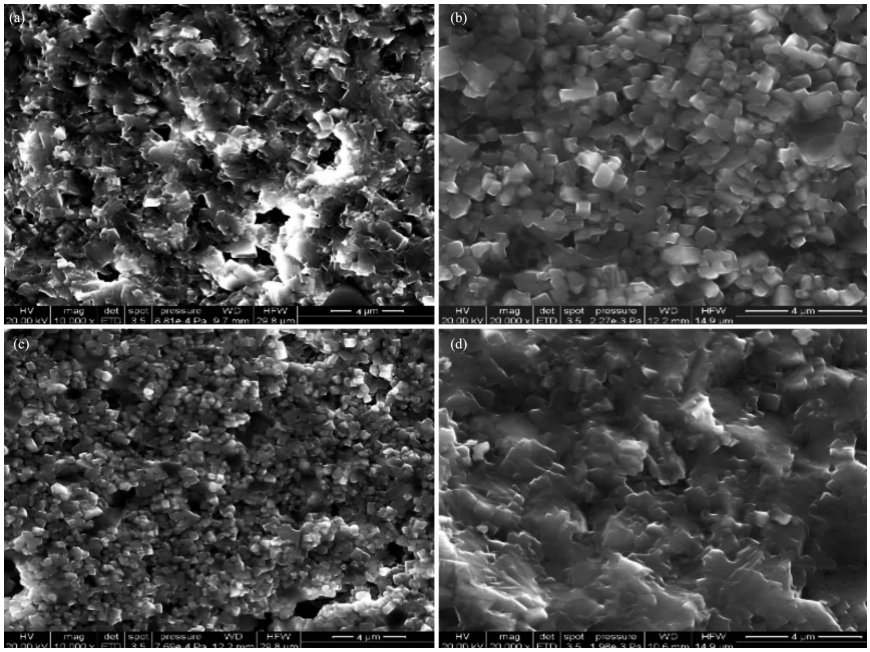

(a) x=1.3; (b) x=1.5; (c) x=1.7; and (d) x=1.9

Fig.3 Fracture surface of $Li_xAl_{x-1}Ge_{3-x}(PO_4)_3$ (x=1.1~1.9) glass ceramics treated at 1123 K for 8 h

microstructure and uniform distribution of the crystals.

The total resistance R_t of the $Li_xAl_{x-1}Ge_{3-x}(PO_4)_3$ (x=1.1~1.9) glass ceramics treated at 1 123 K for 8 h are obtained via the room temperature complex impedance plots. And, the total conductivity (σ_t) of LAGP glass ceramics is calculated (shown in Fig.4) by $\sigma_t=H/(S\cdot R_t)$, where H is the samples thickness and S is the samples surface area. The conductivity increases with the initial increase in x, reaches a maximum value of 5.3×10^{-4} S·cm^{-1} at around x=1.5 and then decreases. This is due to the formation of $Li_4P_2O_7$ and $AlPO_4$ phases (shown in Table 2), which are electrically insulating (dielectric) phases and are believed to influence the conductivity of the glass ceramics, even in smaller concentration [13]. All of the $Li_xAl_{x-1}Ge_{3-x}(PO_4)_3$ (x=1.1~1.9) samples exhibit conductivities over 10^{-4} S·cm^{-1}, illustrating that LAGP glass ceramics are promising electrolyte for application in all-solid-state lithium batteries.

Fig.5 shows the cyclic voltammogram for the $Li_{1.5}Al_{0.5}Ge_{1.5}(PO_4)_3$ glass ceramics recorded at room temperature with a scanning rate of 0.5 mV·s^{-1}. The Lithium deposition (Li+e→Li$^+$) and dissolution (Li→Li$^+$+e) are observed in the potential range from 0.5 to

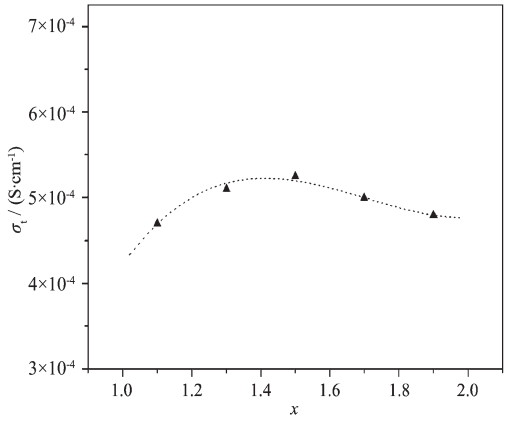

Fig.4 Electrical conductivity of the $Li_xAl_{x-1}Ge_{3-x}(PO_4)_3$ (x=1.1~1.9) glass ceramics

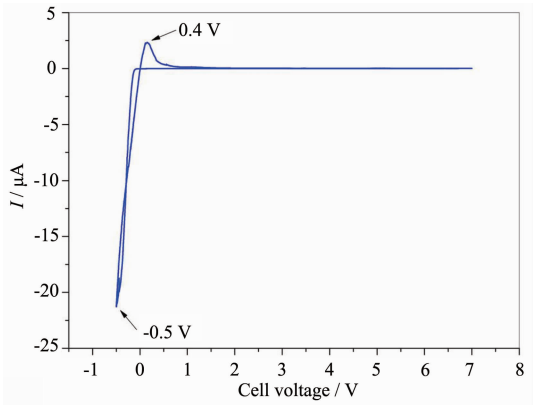

Fig.5 Cyclic voltammogram of $Li_{1.5}Al_{0.5}Ge_{1.5}(PO_4)_3$ glass ceramics

0.4 V. There are no other reactions in the range from 0.5 to 7.2 V versus Li/Li^+, illustrating a wide electrochemical window for LAGP glass ceramics.

3 Conclusions

Lithium ion conducting glass ceramics of $Li_xAl_{x-1}Ge_{3-x}(PO_4)_3$ (x=1.1~1.9) were synthesized and characterized. $LiGe_2(PO_4)_3$ is the dominant crystal phase of LAGP glass ceramics, following by a small quantity of Li_2O crystals as the impurity phase. The total ionic conductivity σ_t reaches a maximum value of 5.3×10^{-4} $S\cdot cm^{-1}$ at room temperature in $Li_{1.5}Al_{0.5}Ge_{1.5}(PO_4)_3$ glass-ceramic with homogeneous crystals distribution, indicating that LAGP glass ceramics are promising electrolyte for application in all-solid-state lithium batteries.

References:

[1] Subramanian M A, Subramanian R, Clearfield A. *Solid State Ionics*, **1986**,**18**:562-569

[2] Aono H, Sugimoto E, Sadaoka Y, et al. *J. Electrochem. Soc.*, **1989**,**136**:590-591

[3] Aono H, Sugimoto E, Sadaoka Y, et al. *J. Electrochem. Soc.*, **1990**,**137**:1023-1029

[4] Cretin M, Fabry P. *J. Electrochem. Soc.*, **1999**,**19**:2931-2940

[5] Bohnke O, Ronchetti P, Mazza D, et al. *Solid State Ionics*, **1999**,**122**:127-136

[6] Maldonado-Manso P, Losilla E R, Martinez-lara M. *Chem. Mater.*, **2003**,**15**:1879-1885

[7] Joykumar S. Thokchom, Binod Kumar. *J. Power Sources*, **2008**,**185**:480-485

[8] Fu Jie. *Solid State Ionics*, **1997**,**104**:191-194

[9] Li S C, Cai J Y, Lin Z X. *Solid State Ionics*, **1988**,**28**:1265-1270

[10]Joykumar S T, Binod K. *J. Power Sources*, **2008**,**185**:480-485

[11]Will G, Powder Diffraction: the Rietveld Method and the Two Stage Method to Determine and Rene Crystal Structures from Powder Diffraction Data, Berlin: Springer-Verlag, **2006**:44-69

[12]Bernardo E, Esposito L, Rambaldi E, et al. *J. Euro. Cera. Soc.*, **2009**,**29**:2921-2927

[13]Joykumar S T, Binod K. *J. Power Sources*, **2010**,**195**:2870-2876